Catalysis Today 177 (2011) 72–78

Contents lists available at ScienceDirect

Catalysis Today

journal homepage: www.elsevier.com/locate/cattod

Mechanism of the catalytic gas-phase aldehyde production from trinuclear W_3S_4 complexes bearing W-OEt groups

Tomás F. Beltrán[a], Marta Feliz[a,b], Rosa Llusar[a,*], Vicent S. Safont[a], Cristian Vicent[c,**]

[a] Departament de Química Física i Analítica, Universitat Jaume I, Av. Sos Baynat s/n, 12071 Castelló de la Plana, Spain
[b] Instituto de Tecnología Química, CSIC-UPV, Avda. De los Naranjos s/n, E-46022 Valencia, Spain
[c] Serveis Centrals dïInstrumentació Cientifica, Universitat Jaume I, Av. Sos Baynat s/n, 12071 Castelló de la Plana, Spain

ARTICLE INFO

Article history:
Received 16 February 2011
Received in revised form 12 May 2011
Accepted 13 May 2011
Available online 22 July 2011

Keywords:
Tungsten clusters
Alkoxo ligands
ESI
CID
Ion-molecule reactions
DFT calculations

ABSTRACT

Collision induced dissociation experiments of the alkoxo $[W_3S_4(dmpe)_2(O)(OCH_2CH_3)]^+$ tungsten (IV) cation reveal that aldehyde elimination is the dominant reaction pathway. Complementary deuterium labelling experiments give support to a hydrogen transfer mechanism, where the hydrogen atom exclusively originates from the α-position of the alkoxo ligand. On the basis of DFT calculations, two competitive mechanisms are proposed: one of them involving a proton transfer from the α-position of the alkoxo ligand to an oxygen atom of the vicinal W=O group; the other corresponding to a hydride transfer mechanism from the α-position of the alkoxo ligand to the geminate tungsten center. The calculated energy profiles show that the former is thermodynamically favoured and the second is kinetically favoured, with small energy differences between the two reaction paths; in consequence, both mechanisms compete under our experimental conditions. The proton transfer mechanism occurs through a seven-membered transition state structure while hydride transfer takes place through a four-center structure defined by the metal and the oxygen, carbon and hydrogen atoms of the ethoxo group.

1. Introduction

Metal oxides are widely used as heterogeneous catalysts for the production of bulk industrial chemicals and are characterized by high selectivities and activities. The basis for such a wide spectrum of applications relies on the variability of oxidation states and rich structural diversity of metal oxides where functional groups such as metal-oxo (M=O), hydroxo (M–OH) or alkoxo (M–OR) are key intermediates involved in the C–H or O–H bond activation processes of organic substrates. For example molybdenum and tungsten oxides are employed in a variety of catalytic reactions that include the selective oxidation of alcohols to aldehydes or the dehydrogenation and isomerization of alkanes [1,2]. However, the mechanistic details of many reactions occurring at the oxide surfaces are not yet fully understood in part due to their irregular composition under real catalytic conditions, so that much effort is being spent to analyse their complex structure and their activity and to subsequently tailored-design improved catalysts in terms of activity and selectivity.

There is a consensus opinion that the surface structure of bulk transition metal oxides can be viewed as an assemblage of polynuclear M_nO_x species, of different n size and n/x stoichiometries, which are considered the simplest model for the interaction of active sites on an oxide surface with organic molecules [3,4]. One way to address the study of these model M_nO_x polynuclear species relies on their transfer to the gas-phase in a controlled environment, and in this context, tandem mass spectrometric techniques have emerged as a promising approach to obtain fundamental insight into the structure and intrinsic reactivity of Mo_nO_x species [5–10].

Schwarz and co-workers reported that gas phase activation of methanol can be achieved by MX_2 (M = Fe, Co, Ni, X = Br, I) species using mass spectrometric techniques. Selective C–H *vs.* O–H bond activation depends on the nature of transition metal M. Iron complexes exhibit an alcohol functional group activation that is explained by the formation of the $[Fe–OCH_3]^+$ gas phase ion. In contrast, nickel complexes showed C–H bond activation by generation of the hydroxymethyl $[Ni–CH_2OH]^+$ cation. Cobalt complexes seem to be less bond selective and both $[Co–CH_2OH]^+$ and $[Co–OCH_3]^+$ are generated in gas phase [11].

Clusters with well defined structures are excellent models for catalytic studies, and size effects seem to be crucial in determining their reactivity. O'Hair's group first demonstrated that dimeric $[Mo_2O_6(OH)]^-$ anions efficiently catalyze the gas-phase

* Corresponding author. Tel.: +34 964728086; fax: +34 964728066.
** Corresponding author. Tel.: +34 964387344; fax: +34 964387309.
E-mail addresses: Rosa.Llusar@qfa.uji.es (R. Llusar), barrera@sg.uji.es (C. Vicent).

0920-5861/$ – see front matter © 2011 Elsevier B.V. All rights reserved.
doi:10.1016/j.cattod.2011.05.017

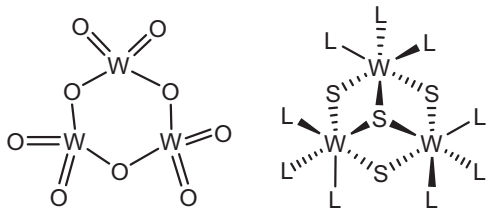

Fig. 1. Proposed structure of the W_3O_9 model catalyst unit (left) and structure of the cuboidal $W_3S_4L_9$ trinuclear cluster (right).

transformation of methanol to formaldehyde while its mononuclear $[MoO_3(OH)]^-$ congener does not [12]. Recently, Schwarz, Schröder et al. have also shown pronounced cluster size effects on the gas-phase reactivity of bare vanadium cluster cations, V_n^+ (n = 1–7), towards methanol [13]. Gas phase tungsten (VI) oxide trimers with a proposed $W_3(\mu\text{-}O)_3O_4$ structure deposited over TiO_2 surfaces have also been investigated as models for the catalytic oxidation of alcohols [14]. In this particular case, 2-propanol is efficiently converted to propene.

During the past decade the research of our group has been focused onto the chemistry of group 6 cluster complexes containing the cuboidal $M_3(\mu_3\text{-}S)(\mu\text{-}S)_3$ core (M = Mo, W), which is topologically related to the $W_3(\mu\text{-}O)_3O_6$ unit, as seen in Fig. 1. These similarities lead us to investigate the activation of alcohols mediated by $W_3(\mu_3\text{-}S)(\mu\text{-}S)_3$ complexes containing terminal hydroxo and oxo groups.

In 2008 we reported the capability of the electrospray ionization (ESI) generated $[W_3S_4(dmpe)_2(OH)O]^+$ cluster species towards methanol activation through formation of methoxo complexes [15]. A combination of deuterium-labelling experiments with computational studies allow us to conclude that activation occurs at the methanol O–H bond which reacts with the hydroxo group of the cluster with the concomitant water release, as represented in Eq. (1).

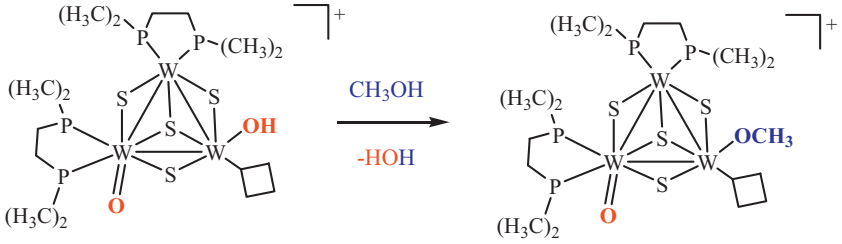

(1)

According to our investigations gas-phase methanol cleavage occurs through a four-electron-four-center mechanism similar to that reported for group six oxides mediated methane activation [16]. The resulting $[W_3S_4(dmpe)_2(OCH_3)O]^+$ species can also be generated in the mass spectrometer in source region by injecting methanol solutions of the hydroxo $[W_3S_4(dmpe)_3(OH)_3]^+$ cluster ion. These in source generated species can be subsequently subjected to collision-induced dissociation experiments to generate formaldehyde. When ethanol solutions of the $[W_3S_4(dmpe)_3(OH)_3]^+$ cation are used instead, the corresponding ethoxo $[W_3S_4(dmpe)_2(OCH_2CH_3)O]^+$ ions are generated. To get a deeper inside on the alcohol activation by these hydroxo W_3S_4 cuboidal complexes we decide to investigate the mechanism of the aldehyde release from the ethoxo $[W_3S_4(dmpe)_2(OCH_2CH_3)O]^+$ complex combining collision induced dissociation experiments with computational studies. The results of this study are presented in this article and they clearly illustrate the potential that arises from combining experimental data with theoretical calculations.

2. Experimental

2.1. General procedures

Compound $[W_3S_4(dmpe)_3(OH)_3]PF_6$ was prepared according to literature procedures [15]. Acetonitrile (HPLC grade, 99.8%), ethanol (HPLC grade, 99.8%), CH_3CD_2OH (98 at.% D) were obtained from Aldrich and used without further purification.

2.2. Mass spectrometry

Electrospray ionization (ESI) and tandem mass experiments were conducted on a Quattro LC (quadrupole–hexapole–quadrupole) mass spectrometer with an orthogonal Z-spray–electrospray interface (Waters, Manchester, UK). Sample solutions were infused via syringe pump directly connected to the ESI source at a flow rate of 10 μL/min and a capillary voltage of 3.5 kV was used in the positive scan mode. The desolvation gas as well as nebulization gas was nitrogen at a flow of 7.5 L/min and 1.3 L/min, respectively. The formation of an assortment of W_3S_4 cations featuring unsaturated tungsten sites as well as alkoxo groups has been previously proved by ion-molecule reactions (IMR) of the hydroxo W_3S_4 cations with alcohols [15]. In the present work, we investigated the formation of these species in the source region to subsequently investigate their characteristic gas phase reactivity via collision induced dissociation (CID) experiments. For this purpose, ESI mass spectra of ethanolic solutions of $[W_3S_4(dmpe)_3(OH)_3]PF_6$ were recorded at high cone voltages (typically U_c 70–100 V) to promote the gas-phase formation of W_3S_4 cations bearing ethoxo groups. CID spectra on the generated ethoxo cluster derivatives were performed with argon at various collision energies, ranging from E_{lab} = 5 to 20 eV. The collision gas pressure was maintained at approximately 6×10^{-4} mbar. The most intense precursor peak of interest was mass-selected with Q1 (isolation width 1 Da), interacted with argon in the hexapole cell while scanning Q2 to monitor the ionic fragments.

2.3. DFT calculations

The theoretical study used $[W_3S_4(PH_3)_4(O)(OCH_2CH_3)]^+$ as molecular model for $[W_3S_4(dmpe)_2O(OCH_2CH_3)]^+$. This made attainable calculation times possible without changing the cluster coordination environment where aldehyde production reaction takes place. The calculations were conducted with the Becke hybrid density functional (B3PW91) [17,18] method as implemented in the Gaussian 03 program suite [19]. Transition metal atoms were represented by the relativistic effective core potential (RECP) from the Stuttgart group and its associated basis set [20], augmented by an f polarization function (Mo: α = 1.043; W: α = 0.823) [21]. P and S atoms were represented by the relativistic effective core potential (RECP) from the Stuttgart group and the associated basis set [22], augmented by a d polarization function (P: α = 0.387; S: α = 0.503) [23]. A 6-31G(d,p) basis set was used for all the other atoms (H, C, O) [24]. The geometry optimizations were performed in gas phase without any symmetry constraint followed by analytical

frequency calculations to confirm that a minimum or a transition state had been reached. The nature of the species connected by a given transition state structure was checked by optimizing to a minima from slightly altered TS geometries along both directions of the transition state vector. We have considered only Gibbs free energies for the discussion, but we provide electronic energies in Supporting Information for all species. In all cases, we have verified that no change of mechanism results from the consideration of Gibbs free energies.

3. Results and discussion

This work is organized as follows: a discussion of the gas-phase elimination of aldehyde from cluster $[W_3S_4dmpe_2(O)(OCH_2CH_3)]^+$ cation upon CID conditions is followed by a description of the plausible reaction mechanisms. For this purpose, isotope-labelling experiments in conjunction with theoretical calculations are employed.

3.1. Gas-phase ESI study of acetaldehyde elimination from $[W_3S_4(dmpe)_2O(OCH_2CH_3)]^+$

Ethoxo $[W_3S_4(dmpe)_2O(OCH_2CH_3)]^+$ species can be easily obtained from ethanolic solutions of salts of the $[W_3S_4(dmpe)_3(OH)_3]^+$ hydroxo cluster under electrospray ionization conditions. Fig. 2 exemplifies the ESI mass spectrum of ethanol solutions of compound $[W_3S_4(dmpe)_3(OH)_3]PF_6$ at high cone voltages where besides the hydroxo species at $m/z = 1013$ and $m/z = 1031$, the corresponding ethoxo-terminated species, at $m/z = 1041$ and $m/z = 1059$ are clearly observed.

CID mass spectrum of mass selected of $[W_3S_4(dmpe)_2O(OCH_2CH_3)]^+$ (m/z 1041) resulted in a mass loss of 44 Da, associated to the elimination of neutral acetaldehyde to give $[W_3S_4(dmpe)_2O(H)]^+$ (see Fig. 3), as represented in Eq. (2). Isotope labelling experiments using deuterated ethanol generates $[W_3S_4(dmpe)_2O(OCD_2CH_3)]^+$ (m/z 1043) under electrospray condition that losses 45 Da when subjected to collision-induced dissociation in the mass spectrometer, as shown in Fig. 3. This is in agreement with a mechanism involving hydrogen transfer from the α-position followed by acetaldehyde elimination (Eq. (3)).

$$[W_3S_4(dmpe)_2O(OCH_2CH_3)]^+ \rightarrow [W_3S_4(dmpe)_2O(H)]^+ + CH_3CHO \quad (2)$$

$$[W_3S_4(dmpe)_2O(OCD_2CH_3)]^+ \rightarrow [W_3S_4(dmpe)_2O(D)]^+ + CH_3CDO \quad (3)$$

O'Hair et al. have observed that the ditungstate $[W_2O_6(OBu)]^-$ anion is unable to generate butanal, in contrast with its molybdenum congener, and that upon collision activation the tungsten anion undergoes non-redox elimination of alkene. The authors attribute this contrasting behaviour to the expected weaker oxidizing power of tungsten species compared to those of molybdenum [12]. Only in the case of the $[W_2O_6(OCH_3)]^-$ anion, for which alkene elimination is not possible due to the absence of a β-hydrogen, formaldehyde elimination has been observed. However, aldehyde elimination is seen for the heterobimetalic $[CrWO_6(OBu)]^-$ anion. These observations indicate that the presence of the stronger oxidant chromium in the mixed metal dinuclear species dominate the tendency of tungsten to eliminate alkene [25]. The trends towards aldehyde elimination observed for the mononuclear trisoxo alkoxo complexes of chromium, molybdenum and tungsten (VI) are also consistent with the expected oxidizing power of the respective metal centers (Cr > Mo > W) [26].

Our results clearly indicate that although the oxidizing power of the metal attached to the alkoxo group is important to determine its selectivity towards aldehyde *vs.* alkene transformation, the nuclearity of the metal model employed also plays a determining role. In particular we have found that trimetallic tungsten (IV) alkoxo complexes selectively generate aldehydes in spite that the oxidizing power of tungsten (IV) is lower than that of tungsten (VI). However, as previously mentioned in the introduction, exclusive formation of propene is observed for the catalytic dehydration of 2-propanol mediated by tungsten trioxide trimers $(WO_3)_3$ (represented in Fig. 1) deposited over silica. At this point it is important to remark that elimination of acetaldehyde from the mass selected gas phase generated $[W_3S_4(dmpe)_2O(OCH_2CH_3)]^+$ cation, requires CID conditions, which is indicative that aldehyde elimination is the rate limiting step in the alcohol activation process.

Two mechanisms are compatible with the experimental and theoretical studies obtained for the aldehyde elimination from the dimolybdate $[Mo_2O_6(OCHR_2)]^-$ anion: (1) transfer of hydrogen from the α-position to an oxo group and two electron reduction of the dimolybdate center, and (2) transfer of hydride from the α-position directly to the metal center. DFT calculations indicate that at least two isomers may result from aldehyde elimination, $[Mo_2{}^{V}O_5(OH)]^-$ and $[HMo_2{}^{VI}O_6]^-$, resulting from mechanisms 1 and 2, respectively. The fact that the catalyst can be regenerated with nitromethane gives support to the first mechanism because no redox reaction is expected for the intermediate in its maximum oxidation state. In contrast, the hydride $[HW_2{}^{VI}O_6]^-$ is exclusively postulated for tungsten based on DFT calculations and its lack of reactivity towards nitromethane [12]. To get a deeper insight

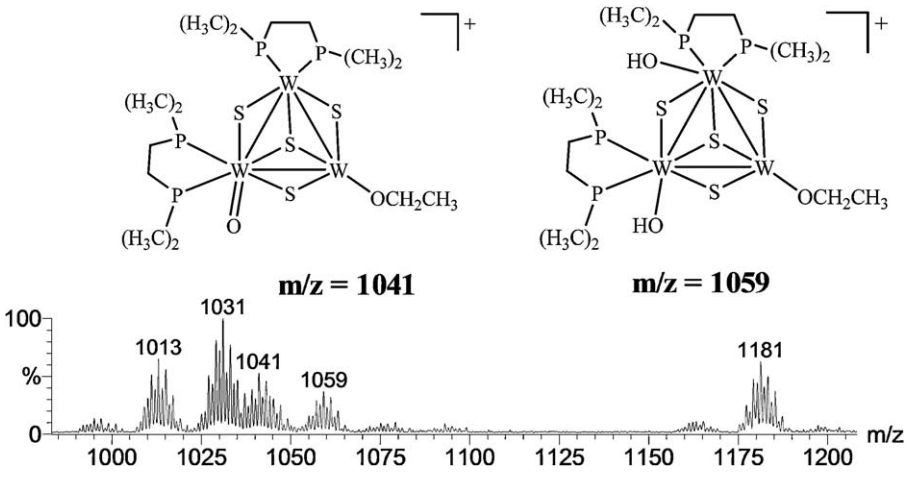

Fig. 2. ESI mass spectrum of $[W_3S_4(dmpe)_3(OH)_3]PF_6$ in ethanol at $U_c = 100$ V.

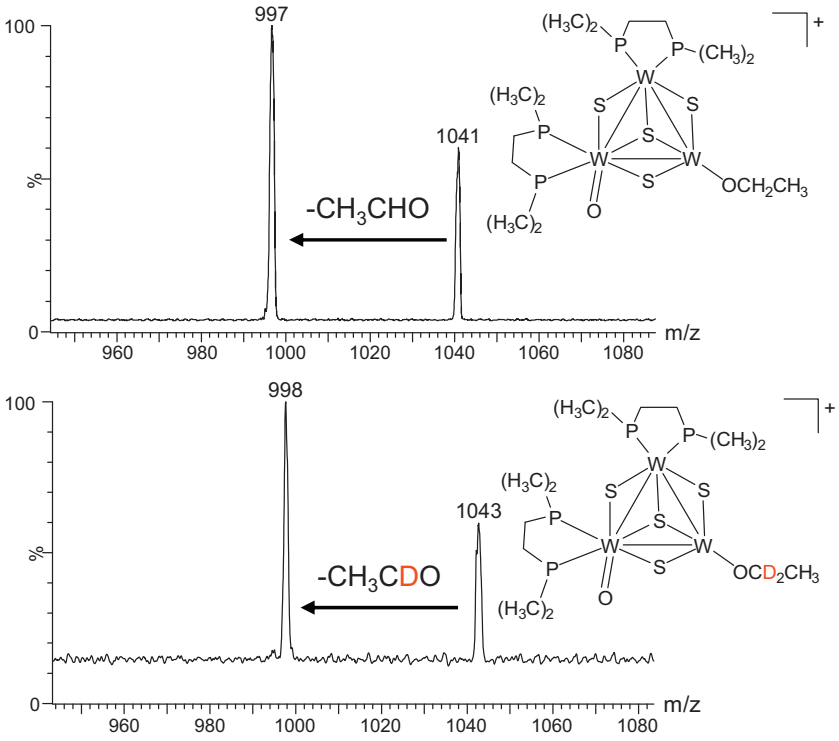

Fig. 3. CID mass spectra of mass-selected $[W_3S_4(dmpe)_2O(OCH_2CH_3)]^+$ (top) and $[W_3S_4(dmpe)_2O(OCD_2CH_3)]^+$ (bottom) recorded at E_{lab} = 15 eV.

into the aldehyde elimination mechanism from the tungsten (IV) $[W_3S_4(dmpe)_2O(OCH_2CH_3)]^+$ cation, we have undertaken a theoretical study using DFT methodologies as detailed in the next section.

3.2. DFT mechanistic study of aldehyde elimination from $[W_3S_4(dmpe)_2O(OCH_2CH_3)]^+$

Calculations were carried out on the model complex $[W_3S_4(PH_3)_4O(OCH_2CH_3)]^+$ where the two diphosphine ligands have been replaced by four monodentated PH_3 phosphines, a common simplification in this kind of systems [27–29]. Two different isomers very close in Gibbs free energy to each other (ca. 0.5 kcal mol^{-1}), represented in Fig. 4, have been found. The mechanisms for the acetaldehyde elimination from both isomers are analysed in the present work.

As previously mentioned, acetaldehyde elimination from $[W_3S_4(dmpe)_2O(OCH_2CH_3)]^+$ is the only observed channel in our CID experiments. The process is represented in Eq. (4).

$$\underset{\mathbf{R}}{[W_3S_4(dmpe)_2O(OCH_2CH_3)]^+} \xrightarrow[-OCHCH_3]{CID} \underset{\mathbf{P}}{[W_3S_4(dmpe)_2O(H)]^+} \quad (4)$$

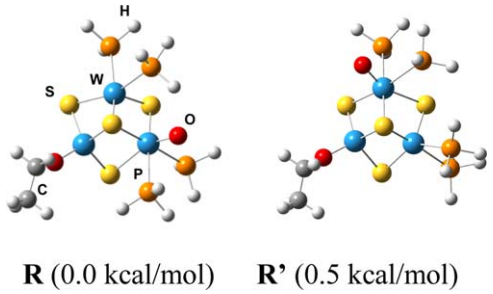

R (0.0 kcal/mol) **R'** (0.5 kcal/mol)

Fig. 4. B3PW91 optimized geometries and relative Gibbs free energies for the two most stable $[W_3S_4(PH_3)_4O(OCH_2CH_3)]^+$ isomers.

Different structures are compatible with the experimental $[W_3S_4(dmpe)_2O(H)]^+$ formulation. Scheme 1 shows the six more stable $[W_3S_4(PH_3)_4O(H)]^+$ isomers (labelled as P followed by a number). A prime symbol is used for the cluster products (**P′**) arising from **R′**. All structures have been calculated as singlet ground states. Calculated energies for the triplet and quintuplet ground states are higher and we have focused our study on the fundamental singlet state.

Optimized structures for **P1** and **P1′** present a marked distortion from an equilateral triangle disposition of the metal centers, with two metal–metal distances between 2.7 and 2.8 Å and a third one close to 2.4 Å. Longer distances are marked with discontinuous lines in Scheme 1. The metal–oxygen bond lengths for **P1** and **P1′** are 1.939 and 1.949 Å, respectively, similar to those reported from X-ray data for tungsten–hydroxo cluster compounds [27]. The three metal atoms in **P2**, **P2′**, **P3** and **P3′** define a less distorted triangle with tungsten–tungsten distances ranging between 2.63 and 2.95 Å. The longer metal–metal distance is found for the bond approximately *trans* to the W=O group in the **P3′** structure. The equivalent bond lengths in **P2**, **P2′** and **P3** are 2.83, 2.94 and 2.81 Å, respectively. The values of the W=O distances in **P2**, **P2′**, **P3** and **P3′**, between 1.71 and 1.75 Å, agree with its double bond character. The higher metal–sulphur distance deviations are associated to the W–μ-S bonds, where the bond lengths vary from 2.3 to 2.6 Å for all the structures. In **P1** and **P1′**, the longest length corresponds to the W–μ-S bond linking the sulphur atom with the unsaturated $W(PH_3)_2$ group, and in **P2** the longest length corresponds with the W–μ-S bond *trans* to the metal-oxo group.

Structures **P1** and **P1′** are compatible with a proton transfer reaction mechanism, while the remaining structures correspond to a hydride transfer mechanism. These mechanisms parallel those reported by O'Hair for the aldehyde elimination by alkoxo dimolybdenum species, mentioned in the previous section [12]. Fig. 5 presents the different energetic profiles linking the reactants (**R** or **R′**) with the cluster products (**P** and **P′**) plus acetaldehyde. Relevant numerical values are listed in Table 1. All transition

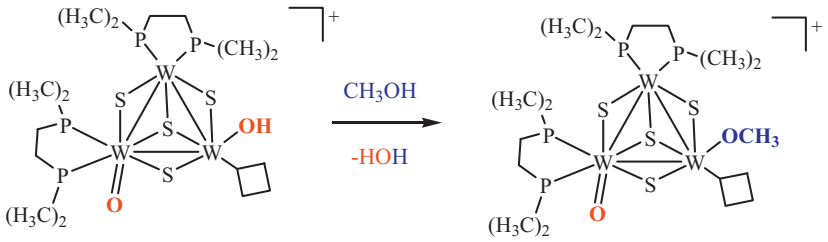

Scheme 1. Simplified structures, and relative (to **R**) Gibbs free energies (kcal mol^{-1}), of the products of acetaldehyde elimination from **R** (top) and **R′** (bottom). The key oxygen and hydrogen atoms have been highlighted in red. The stereochemistry around one of the tungsten centers is shown for **P1**. (For interpretation of the references to colour in this scheme legend, the reader is referred to the web version of the article.)

structures (labelled as TS) connecting **R** and **R′** with their corresponding products have been calculated except for **P1**. In this case the stereochemistry of **R** made the transition state calculation unfeasible for a hydrogen transfer mechanism due to the large separation between the α-hydrogen at the ethoxo moiety with respect the oxo group. An inspection of the thermodynamics shows that conversion of **R** and **R′** into **P1** or **P1′** (mechanism 1) plus acetaldehyde are endothermic processes. In the case of mechanism 2, the energies corresponding to the formation of **P2′** and **P3′** hydrides are 6.2 and 16.3 kcal mol^{-1}, respectively, higher than reaction energy for **P1′**. Similarly, the reaction energies for obtaining **P2** or **P3** hydrides are 1.1 kcal mol^{-1} lower and 7.2 kcal mol^{-1} higher than the reaction energy for **P1**. These results show that in all cases the hydrogen transfer reactions are endothermic, and the most thermodynamically favourable processes are associated to the formation of the **P1′**, **P1** and **P2** cluster products. In spite of the endothermic character calculated for all reactions, the high energetic experimental conditions are sufficient to generate acetaldehyde in the collision cell.

All transition structures (TS) are linked to the cluster products **P** and **P′** through intermediate adducts (labelled as PC), as illustrated in Fig. 5. In the structure of these intermediates, the carbonylic oxygen of the leaving aldehyde interacts with the tungsten atom to which the ethoxo group was formally bound. In a following step along the reaction coordinate, the acetaldehyde leaves causing an increase in the free energy. Although the acetaldehyde departure causes an entropy increase, and this fact would reduce the Gibbs free energy, the enthalpic term dominates, and a net increase in Gibbs free energy has been calculated for the acetaldehyde departure steps.

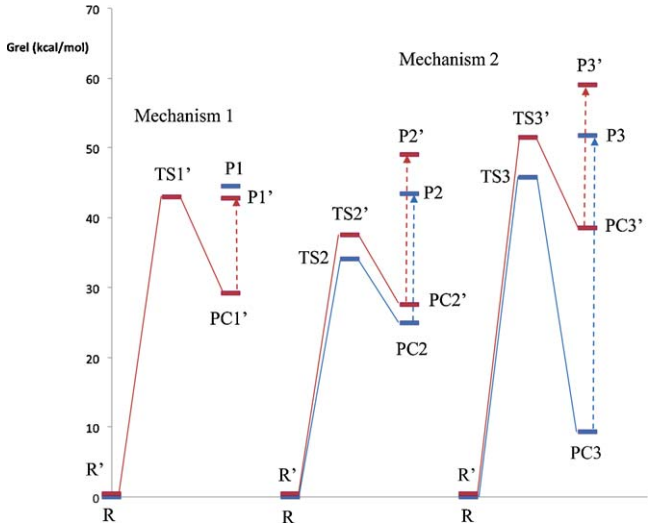

Fig. 5. Energetic profiles linking the reactants (**R** or **R′**) with the products (**P** and **P′**) plus acetaldehyde. The relative Gibbs free energies are calculated with respect to the **R** energy.

Regarding the study of the intramolecular hydrogen transfer mechanisms, only one transition structure has been obtained for each of the reactions described above. For the thermodynamically most favourable reactions previously described, **TS1′** and **TS2** have been optimized as transition states (see Fig. 6). As mentioned above, the putative TS associated to the hydrogen transfer from **R** to **P1** could not be found because of the high interatomic distance between the reaction centers.

TS1′ is associated to the α-hydrogen transfer from alkoxo ligand to W=O to give **PC1′**, where **PC1′** is the adduct between RC=O and the tungsten center, as explained. Similar α-hydrogen abstraction mechanisms from an alkoxo ligand by neighboring terminal M=O centers have been described by other authors for molybdenum complexes [12,30,31]. On the other hand, **TS2** corresponds to an α-hydrogen transfer from the alkoxo ligand to the tungsten atom in geminal position to give the **PC2** adduct. A similar mechanism has been reported by Gregoriades et al. for the study of methanol to formaldehyde oxidation on mononuclear models of silica-supported molybdenum [31]. Activation free energies of **TS1′** and **TS2** (see Fig. 5) show that α-hydrogen transfer to geminate tungsten atom is 8.4 kcal mol^{-1} lower. However, the thermodynamics of the reaction shows an opposite trend: formation of **P1′** is 1.1 kcal mol^{-1} more favourable than formation of **P2**. On the other hand, the energies of the product adducts, 25.0 (**PC2**) and 29.2 kcal mol^{-1} (**PC1′**), are close to each other.

From these results, we can conclude that the preferred processes are associated to a proton transfer from alkoxo ligand to the W=O group through a **TS1′** transition state to give **P1′** and acetaldehyde, and to a hydride transfer to the geminate tungsten center via the **TS2** transition structure to give **P2** and acetaldehyde.

A more detailed description of the transition structures, shows that the transition state eigenvector of **TS1′** represents a hydrogen transfer to a vicinal W=O group, with an imaginary frequency of $\nu = 1495i\,cm^{-1}$. An inspection of the geometry of **TS1′** shows a seven-membered transition state structure, similar to that reported by Goddard III in the study of the α-hydrogen abstraction reaction

Table 1
Relative Gibbs free energies (G) to **R** (kcal mol^{-1}). Reaction energies (G_R) and activation energies ($\Delta G^{\neq}$) are also given in kcal mol^{-1}.

Species	G	G_R	$\Delta G^{\neq}$	Species	G	G_R	$\Delta G^{\neq}$
R	0.0			**R′**	0.5		
TS1	–			**TS1′**	43.0		42.5
PC1	–			**PC1′**	29.2	28.7	
P1	44.5	44.5		**P1′**	42.8	42.3	
TS2	34.1		34.1	**TS2′**	37.5		37.0
PC2	25.0	25.0		**PC2′**	27.6	27.1	
P2	43.4	43.4		**P2′**	49.0	48.5	
TS3	45.8		45.8	**TS3′**	51.5		51.0
PC3	9.3	9.3		**PC3′**	38.5	38.0	
P3	51.7	51.7		**P3′**	59.1	58.6	

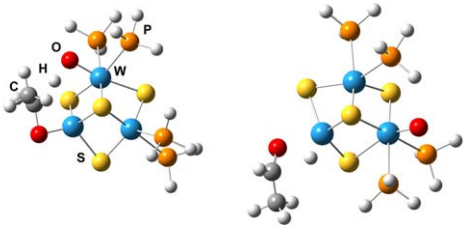

TS1' (42.5 kcal mol^{-1}) **TS2** (34.1 kcal mol^{-1})

Fig. 6. Optimized geometries for **TS1**′ and **TS2**, and corresponding activation free energies associated to α-hydrogen migration.

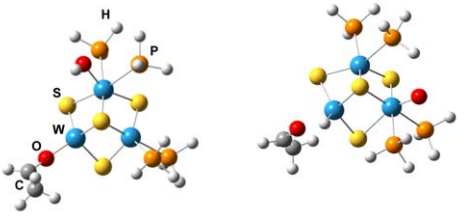

PC1' (28.7 kcal mol^{-1}) **PC2** (25.0 kcal mol^{-1})

Fig. 7. Optimized geometries and reaction free energies of **PC1**′ and **PC2** intermediates.

in $Mo_3O_8(OCH_2CHCH_2)$ [30]. The O–H distance in the forming bond is 1.244 Å, while the α-C–H distance has increased from 1.095 in **R**′ to 1.483 Å. The C–O bond distance slightly increases, from 1.428 to 1.461 Å, keeping the sp^3 nature of the C–O alkoxo bond. These bond distances indicate that the hydrogen abstraction is almost complete in **TS1**′. Moreover, the W–O bond at the acetaldehyde formation site elongates from 1.836 to 1.871 Å while the W=O bond at the hydrogen accepting site elongates from 1.744 to 1.845 Å, which is consistent with the transformation of a W–O σ-bond to a O → W coordination, and of a W–O π-bond to a W–O σ-bond, respectively. Furthermore, the distance between the two reduced tungsten atoms slightly decreases from 2.794 to 2.670 Å, and the remaining intermetallic distances do not show important changes.

In the case of **TS2**, the eigenvector represents a hydrogen transfer to a geminate W atom (with an imaginary frequency of $\nu = 97.3i\,cm^{-1}$) in a four-center structure defined by the metal, the oxygen, carbon and hydrogen atoms from the ethoxo moiety. An analysis of the interatomic distances shows that the α-C–H distances of the ethoxo group elongates from 1.097 in **R** to 2.222 Å in **TS2** and the W–O bond increases from 1.843 to 2.159 Å. The W–H bond in the acetaldehyde formation reaction decreases from 3.484 to 1.756 Å. It is worth noting that in this case, the C–O bond distance decreases from 1.428 in **R** to 1.257 Å, in agreement with the development of sp^2 character of the reactive carbon–oxygen bond. Regarding to the intermetallic distances, no substantial changes are observed.

An inspection of the geometries of the intermediates, **PC1**′ and **PC2**, illustrated in Fig. 7, shows W–O interatomic distances of 1.931 and 2.142 Å for **PC1**′ and **PC2**, respectively, which are associated to a O → M donor interaction.

The C=O bonds for **PC1**′ and **PC2** show distances of 1.270 and 1.234 Å, respectively, characteristic of aldehyde compounds. In the case of **PC2**, the W–H interatomic distance of 1.720 Å is usual for DFT optimized metal–hydride bonds in tungsten cluster compounds [27,28,32]. With regard to the intermetallic distances of **PC1**′, the distance between the two reduced tungsten atoms elongates in 0.158 Å from **TS1**′ to **PC1**′. This distance becomes the longest, and the remaining W–W bonds are ca. 2.78 Å. In relation to the intermetallic distances for **PC2**, no substantial changes are observed between **TS2** and **PC2**.

4. Conclusion

The picture that is emerging from collision induced dissociation experiments of the alkoxo $[W_3S_4(dmpe)_2(O)(OCH_2CH_3)]^+$ tungsten (IV) cation reveals acetaldehyde elimination is the dominant reaction pathway. This process consists in a hydrogen transfer mechanism, in which the hydrogen atom exclusively originates from the α-position of the alkoxo ligand. On the basis of DFT calculations, two competitive mechanisms are proposed: one of them involving a proton transfer from the α-position of the alkoxo ligand to an oxygen atom of the vicinal W=O group; the other corresponding to a hydride transfer mechanism from the α-position of the alkoxo ligand to the geminate tungsten center. The energy profiles point out that the former is thermodynamically favoured and the latter is kinetically favoured, with small energy differences between the two reaction paths; in consequence, both mechanisms are competitive under our experimental conditions.

Acknowledgments

The financial support of the Spanish Ministerio de Ciencia e Innovación (research projects CTQ2008-02670 and CTQ2009-14541-C02-01), Fundació Bancaixa-UJI (P1.1B2008-37 and P1.1B2010-46), and Generalitat Valenciana (ACOMP/2011/037) and Prometeo/2009/053) is gratefully acknowledged. The authors also thank the Servei Central d'Instrumentació Cientifica (SCIC) and the Servei d'Informàtica of the Universitat Jaume I for providing us with spectrometric facilities, and with computing time. T.F.B. thanks the Spanish Ministerio de Ciencia e Innovación (MICINN) for a doctoral fellowship (FPI).

Appendix A. Supplementary data

Supplementary data associated with this article can be found, in the online version, at doi:10.1016/j.cattod.2011.05.017.

References

[1] A.P.V. Soares, M.F. Portela, Catal. Rev.: Sci. Eng. 47 (2005) 125–174.
[2] Y. Ono, Catal. Today 81 (2003) 3–16.
[3] G.E. Johnson, R. Mitric, V. Bonacic-Koutecky, A.W. Castleman, Chem. Phys. Lett. 475 (2009) 1–9.
[4] E.L. Muetterties, Science 196 (1977) 839–848.
[5] J. Roithova, D. Schroder, Coord. Chem. Rev. 253 (2009) 666–677.
[6] R.A.J. O'Hair, Chem. Commun. (2006) 1469–1481.
[7] J. Roithova, D. Schroder, H. Schwarz, Angew. Chem. Int. Ed. 44 (2005) 3092–3096.
[8] P.B. Armentrout, Eur. J. Mass Spectrom. 9 (2003) 531–538.
[9] K.A. Zemski, D.R. Justes, A.W. Castleman, J. Phys. Chem. B 106 (2002) 6136–6148.
[10] S. Gronert, Chem. Rev. 101 (2001) 329–360.
[11] M. Schlangen, H. Schwarz, ChemCatChem 2 (2010) 799–802.
[12] T. Waters, R.A.J. O'Hair, A.G. Wedd, J. Am. Chem. Soc. 125 (2003) 3384–3396.
[13] S. Feyel, D. Schröder, H. Schwarz, J. Phys. Chem. A 113 (2009) 5625–5632.
[14] Y.K. Kim, R. Rousseau, B.D. Kay, J.M. White, Z. Dohnalek, J. Am. Chem. Soc. 130 (2008) 5059–5061.
[15] C. Vicent, M. Feliz, R. Llusar, J. Phys. Chem. A 112 (2008) 12550–12558.
[16] G. Fu, X. Xu, H.L. Wan, Catal. Today 117 (2006) 133–137.
[17] A.D. Becke, J. Chem. Phys. 98 (1993) 5648–5652.
[18] J.P. Perdew, Y. Wang, Phys. Rev. B 45 (1992) 13244–13249.
[19] M.J. Frisch, G.W. Trucks, H.B. Schlegel, G.E. Scuseria, M.A. Robb, J.R. Cheeseman, J.A. Montgomery, T. Vreven, K.N. Kudin, J.C. Burant, J.M. Millam, S.S. Iyengar, J. Tomasi, V. Barone, B. Mennucci, M. Cossi, G. Scalmani, N. Rega, G.A. Petersson, H. Nakatsuji, M. Hada, M. Ehara, K. Toyota, R. Fukuda, J. Hasegawa, M. Ishida, T. Nakajima, Y. Honda, O. Kitao, H. Nakai, M. Klene, X. Li, J.E. Knox, H.P. Hratchian, J.B. Cross, V. Bakken, C. Adamo, J. Jaramillo, R. Gomperts, R.E. Stratmann, O. Yazyev, A.J. Austin, R. Cammi, C. Pomelli, J.W. Ochterski, P.Y. Ayala, K. Morokuma, G.A. Voth, P. Salvador, J.J. Dannenberg, V.G. Zakrzewski, S. Dapprich, A.D. Daniels, M.C. Strain, O. Farkas, D.K. Malick, A.D. Rabuck, K. Raghavachari,

J.B. Foresman, J.V. Ortiz, Q. Cui, A.G. Baboul, S. Clifford, J. Cioslowski, B.B. Stefanov, G. Liu, A. Liashenko, P. Piskorz, I. Komaromi, R.L. Martin, D.J. Fox, T. Keith, M.A. Al-Laham, C.Y. Peng, A. Nanayakkara, M. Challacombe, P.M.W. Gill, B. Johnson, W. Chen, M.W. Wong, C. Gonzalez, J.A. Pople, Gaussian 03 Revision D.02, Gaussian Inc., Wallingford, CT, 2004.
[20] D. Andrae, U. Haussermann, M. Dolg, H. Stoll, H. Preuss, Theor. Chim. Acta 77 (1990) 123–141.
[21] A.W. Ehlers, M. Bohme, S. Dapprich, A. Gobbi, A. Hollwarth, V. Jonas, K.F. Kohler, R. Stegmann, A. Veldkamp, G. Frenking, Chem. Phys. Lett. 208 (1993) 111–114.
[22] A. Bergner, M. Dolg, W. Kuchle, H. Stoll, H. Preuss, Mol. Phys. 80 (1993) 1431–1441.
[23] A. Hollwarth, M. Bohme, S. Dapprich, A.W. Ehlers, A. Gobbi, V. Jonas, K.F. Kohler, R. Stegmann, A. Veldkamp, G. Frenking, Chem. Phys. Lett. 208 (1993) 237–240.
[24] Harihara Pc, J.A. Pople, Theor. Chim. Acta 28 (1973) 213–222.
[25] T. Waters, R.A.J. O'Hair, A.G. Wedd, Inorg. Chem. 44 (2005) 3356–3366.
[26] S. Feyel, T. Waters, R.A.J. O'Hair, A.G. Wedd, Dalton Trans. (2004) 4010–4016.
[27] M.G. Basallote, M. Feliz, M.J. Fernandez-Trujillo, R. Llusar, V.S. Safont, S. Uriel, Chem. Eur. J. 10 (2004) 1463–1471.
[28] A.G. Algarra, M.G. Basallote, M. Feliz, M.J. Fernandez-Trujillo, R. Llusar, V.S. Safont, Chem. Eur. J. 12 (2006) 1413–1426.
[29] T.F. Beltrán, M. Feliz, R. Llusar, J.A. Mata, V.S. Safont, Organometallics 30 (2011) 290–297.
[30] S. Pudar, J. Oxgaard, K. Chenoweth, A.C.T. van Duin, W.A. Goddard, J. Phys. Chem. C 111 (2007) 16405–16415.
[31] L.J. Gregoriades, J. Dobler, J. Sauer, J. Phys. Chem. C 114 (2010) 2967–2979.
[32] A.S.G. Algarra, M.G. Basallote, M.J. Fernandez-Trujillo, R. Llusar, V.S. Safont, C. Vicent, Inorg. Chem. 45 (2006) 5774–5784.